Supplementary Material

Capacitive-piezoresistive hybrid flexible pressure sensor based on conductive micropillar arrays with high sensitivity over a wide dynamic range

Zhiran Shen[1,#], Chengduan Yang[1,#], Chuanjie Yao[1,#], Ziqi Liu[1], Xinshuo Huang[1], Zhengjie Liu[1], Jingshan Mo[1], Huihua Xu[2], Gen He[3], Jun Tao[1], Xi Xie[1], Tian Hang[1,*], Hui-Jiuan Chen[1,*], Fanmao Liu[1,*]

[1]The First Affiliated Hospital of Sun Yat-sen University, School of Electronics and Information Technology, State Key Laboratory of Optoelectronic Materials and Technologies, Guangdong Province Key Laboratory of Display Material and Technology, Sun Yat-sen University, 510006 Guangzhou, China

[2]College of Chemistry and Materials Science, Jinan University, 510632 Guangzhou, China

[3]School of Pharmaceutical Sciences, Guangzhou Medical University, 511436 Guangzhou, China

* Corresponding authors: Tian Hang, hangtian@mail.sysu.edu.cn; Hui-Jiuan Chen, chenhuix5@mail.sysu.edu.cn; Fanmao Liu, liufm9@mail.sysu.edu.cn

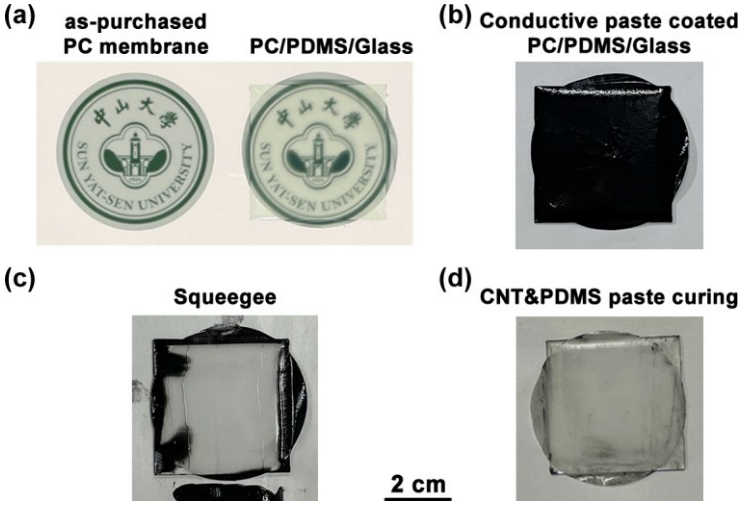

Figure S1. Photographs of (a) PC membrane filters attached on glass substrate (the as-purchased PC membrane was used for comparison), (b) conductive paste spin-coated on the PC membrane, (c) scraping process to remove extra conductive paste, (d) PC membrane after scraping process.

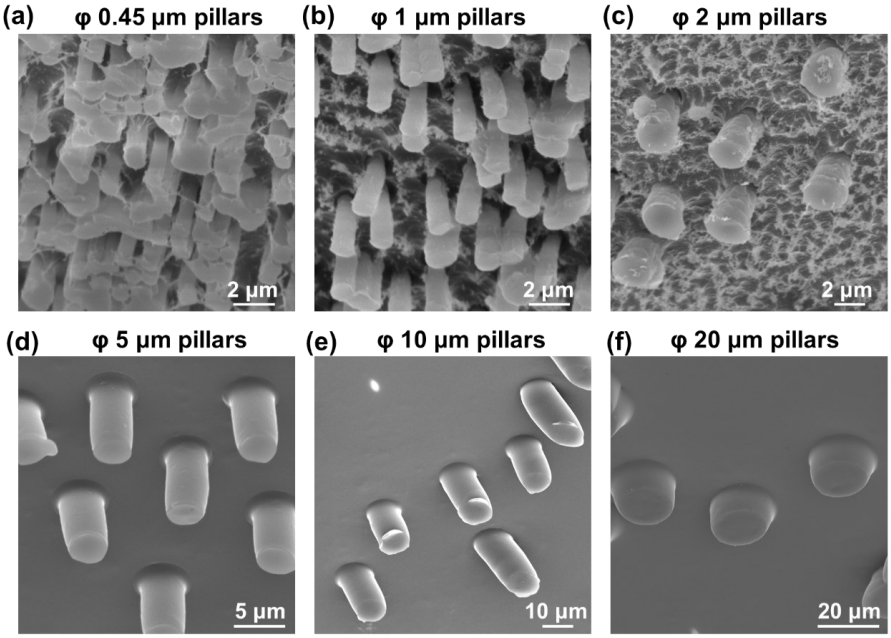

Figure S2. Micropillar arrays with various diameters, including (a) 0.45 μm, (b) 1 μm, (c) 2 μm, (d) 5 μm, (e) 10 μm and (f) 20 μm. All micropillar arrays were fabricated based on track-etched PC membranes, which contain pores with densities of 1×10^8, 2×10^7, 2×10^6, 4×10^5, 1×10^5 and 4×10^4 pores/cm^2, respectively.

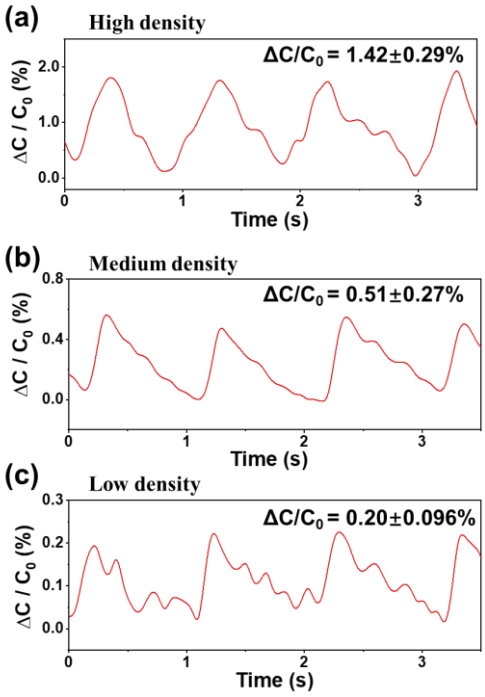

Figure S3. Influence of the pillar-density on the pulse monitoring performance. A batch of MAPS were fabricated using the same template (1-μm-pore-size PC membrane), same etching time (1.5 h), but different spin-coating speed (2000, 1000, 500 rpm for 60s). The obtained micropillar arrays presented different pillar-densities as demonstrated in **Figure 2d**. Their performance of monitoring arterial pulses was showed in (a-c). The results indicate that higher pillar-density would lead to larger electro-mechanical response ($\Delta C/C_0$), under some specific premises.

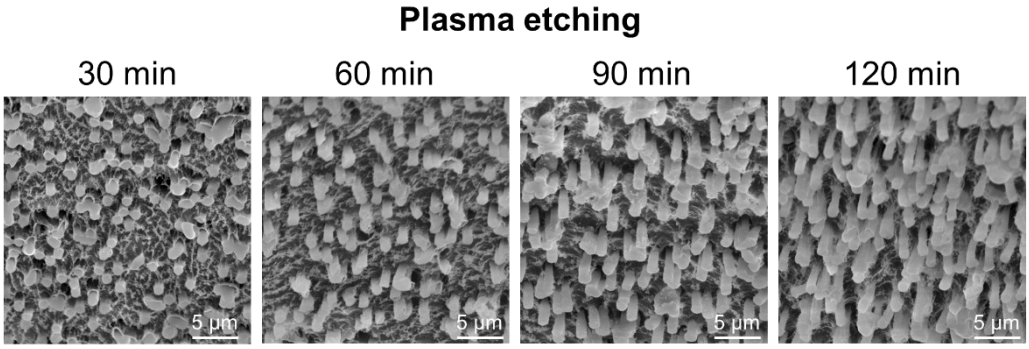

Figure S4. Controlling the length of pillars by adjusting the plasma etching time. Pillars are with the diameter of 1 μm. 30 – 120 min etching can produce pillars with the length from ~1 μm to ~5 μm.

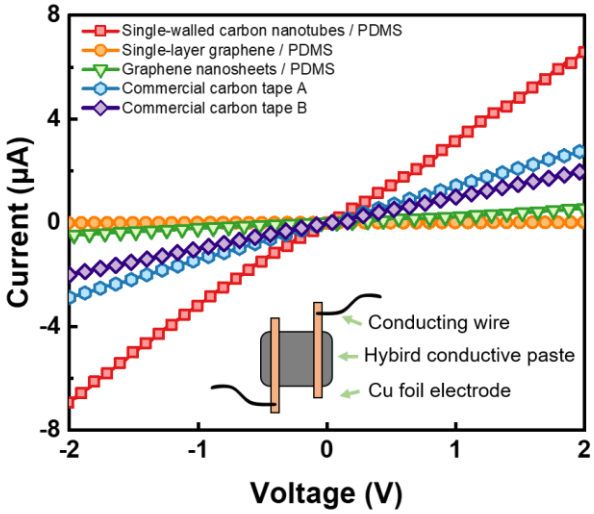

Figure S5. Comparison of *I-V* characteristics of carbon-material/PDMS conductive pastes. The inset illustrated the measuring method. All the pastes were fabricated in the same sizes and affixed uniformed Cu foli electrodes with conducting wires. Commercial conductive carbon tapes were tested as reference standards.

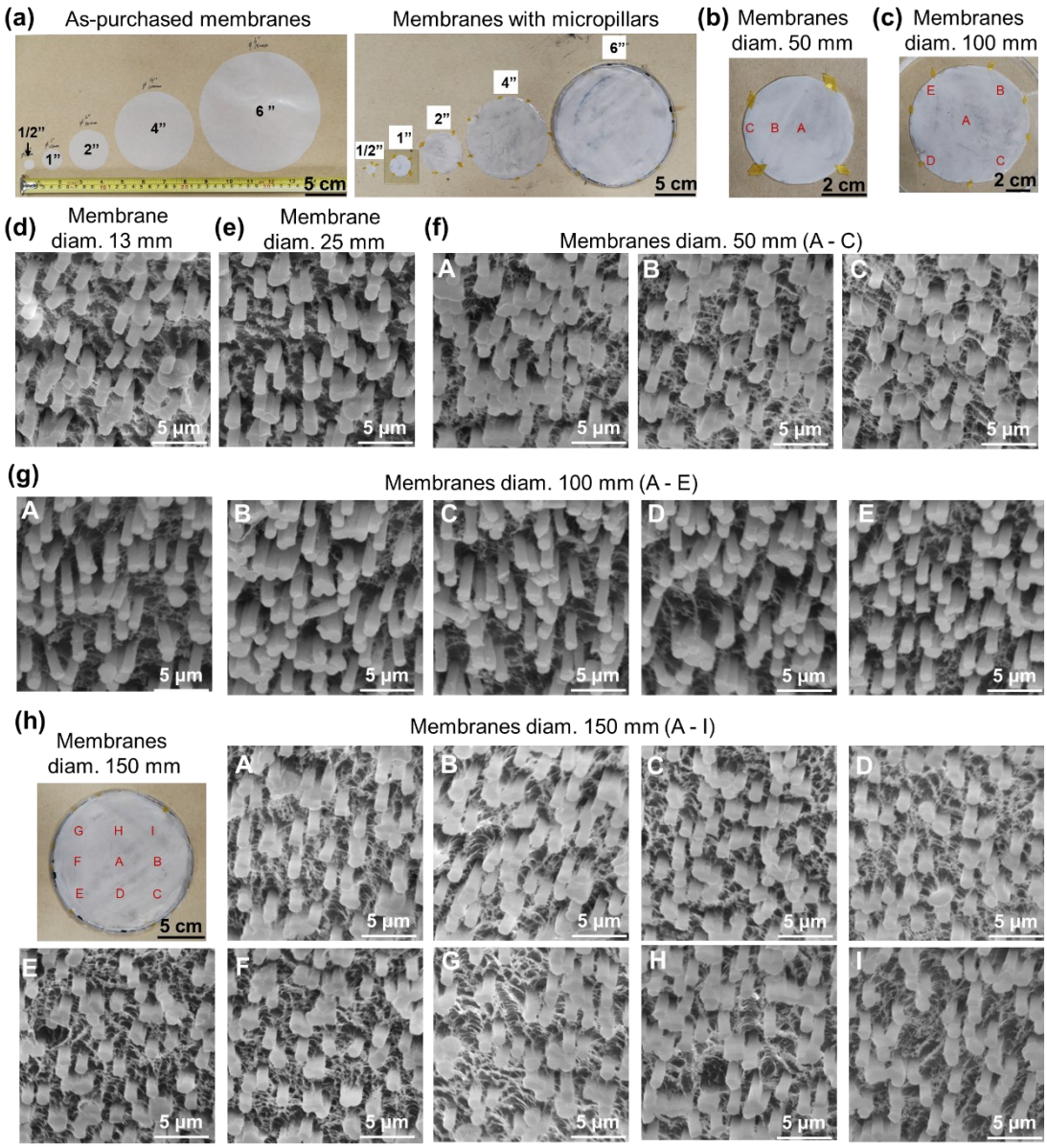

Figure S6. Preliminary verification of the batch production capability of the micropillar arrays based on track-etched membranes. (a) As-purchased track-etched membranes and processed membranes with micropillar arrays. All membranes are with the pore size of 1 µm. Diameters of membranes are 13 mm (1/2”), 25 mm (1”), 50 mm (2”), 100 mm (4”) and 150 mm (6”), respectively. Centers of 13-mm and 25-mm membranes were sampled for SEM characterizations, as shown in (d) and (e). Center and peripheral areas of 50-mm, 100-mm and 150-mm membranes were sampled, as marked in (b), (c) and the first panel of (h). Corresponding SEM images were showed in panels A-C in (f), panels A-E in (g) and panels A-I in (h). The results verified the feasibility of fabricating large-area micropillar arrays based on track-etched membranes, and demonstrated the morphological uniformity of achieved membranes, indicating the potential of the batch production of conductive-micropillar-arrays based pressure sensors.

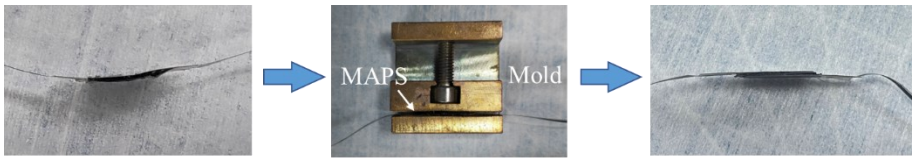

Figure S7. Hot-pressing process to permanently flatten the MAPS. The curved sensor was compressed in the hot-pressing mold and kept flattened. Then they were heated up to 120°C in a drying oven for 1 hour. After the hot-pressing process, the flattened sensor was obtained.

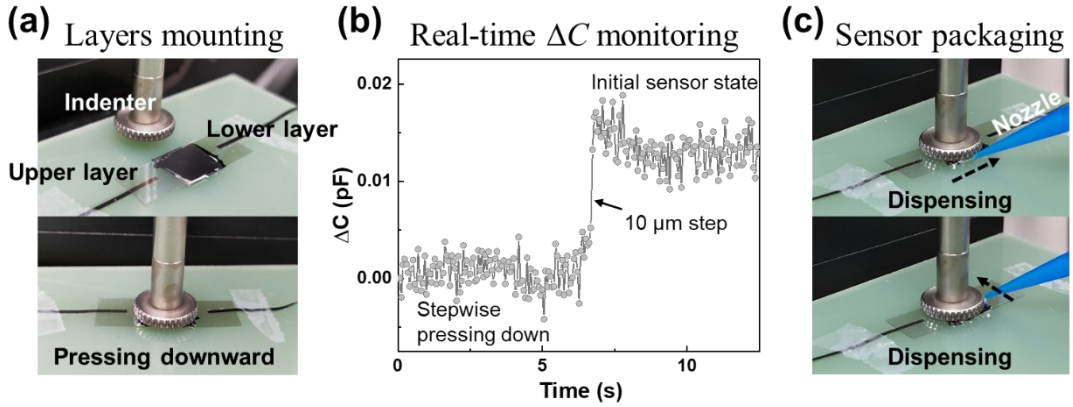

Figure S8. Precise control of the sensor assembly/packaging process. (a) Two layers with the stacking of flexible electrode/conductive paste/micropillar arrays were mounted face to face, and the wires were connected to the LCR meter for a real-time monitoring of capacitance. An indenter with a diameter of 1/2 inch was mounted on the electric translation stage and pressed downward stepwise. (b) The real-time monitored capacitive variation while the indenter pressed down. As demonstrated, no capacitive response was detected before the threshold, though the indenter was pressing down with steps of 100 – 10 μm, which indicated the upper and lower layers were not close enough. ΔC presented a sudden increase when the distance between the layers reached the threshold, and it stayed at the plateau. This state was defined as the "initial sensor state" and ceasing the pressing. Considering the sampling rate and the amplitude resolution of the LCR meter, pressing steps smaller than 10 μm were not employed. (c) At the "initial sensor state", Ecoflex (item 00-50) was dispensed to seal the edges of the contacted two layers, along two edges as marked by the dashed arrows. Ecoflex 00-50 possesses a fast pot time (18 min) and cure time (3 h), thus the sensor and the indenter were kept at the "initial sensor state" for 20 min and then carefully separated. The other two edges were sealed by dispensing subsequently, then the assemblies were stored at room temperature for 3 hours to obtain the MAPS.

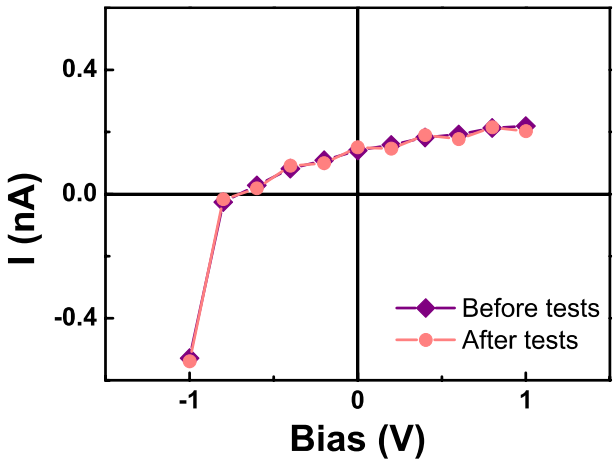

Figure S9. *I-V* characteristics of one MAPS before and after the compress tests.

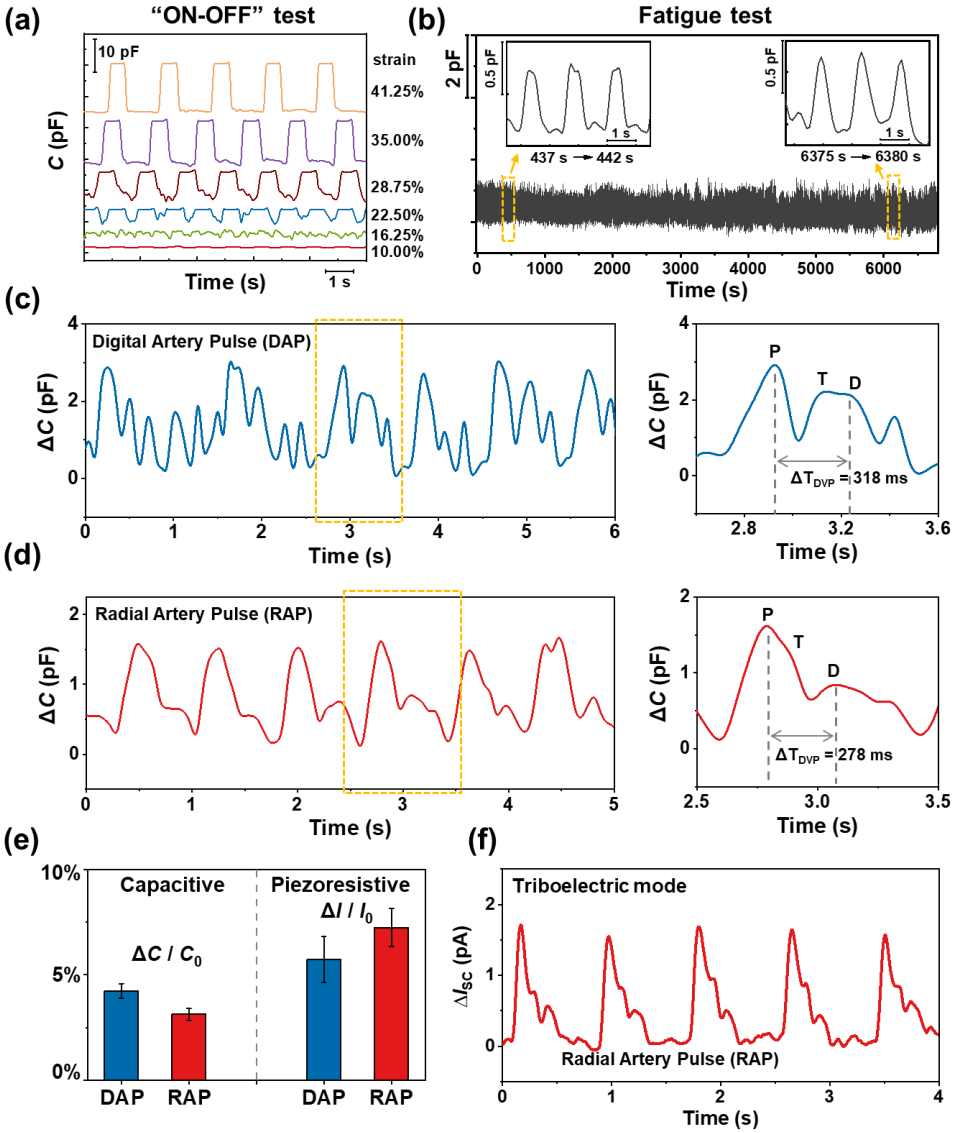

Figure S10. Characterizing the MAPS in capacitive mode. AC source of 1 V oscillation at 10 kHz were employed. The sample used for evaluating fundamental performance and demonstrating applications (Figure 3-5) was employed here. (a) "ON-OFF" responses of the MAPS. (b) Fatigue properties of the MAPS. More than 4000 cycles were performed from 0 to 28.75% strain. (c,d) Respective capacitive response of the DAP and the RAP collected from a seated healthy subject. Representative waveforms were annotated by the yellow dashed frames and zoomed at the right panels. Characteristic waveforms (P, T, D) and the ΔT_{DVP} were annotated in the zoomed panels. (e) Normalized intensity of pulse signals monitored by the MAPS in capacitive ($\Delta C / C_0$) and piezoresistive ($\Delta I / I_0$) modes. In the case of the same sample and subject, the piezoresistive mode outputted stronger signals than the capacitive mode, in both the DAP and RAP monitoring. (f) Monitoring the RAP in the triboelectric mode. Short-circuit current (I_{sc}) was recorded and its variation was plotted.

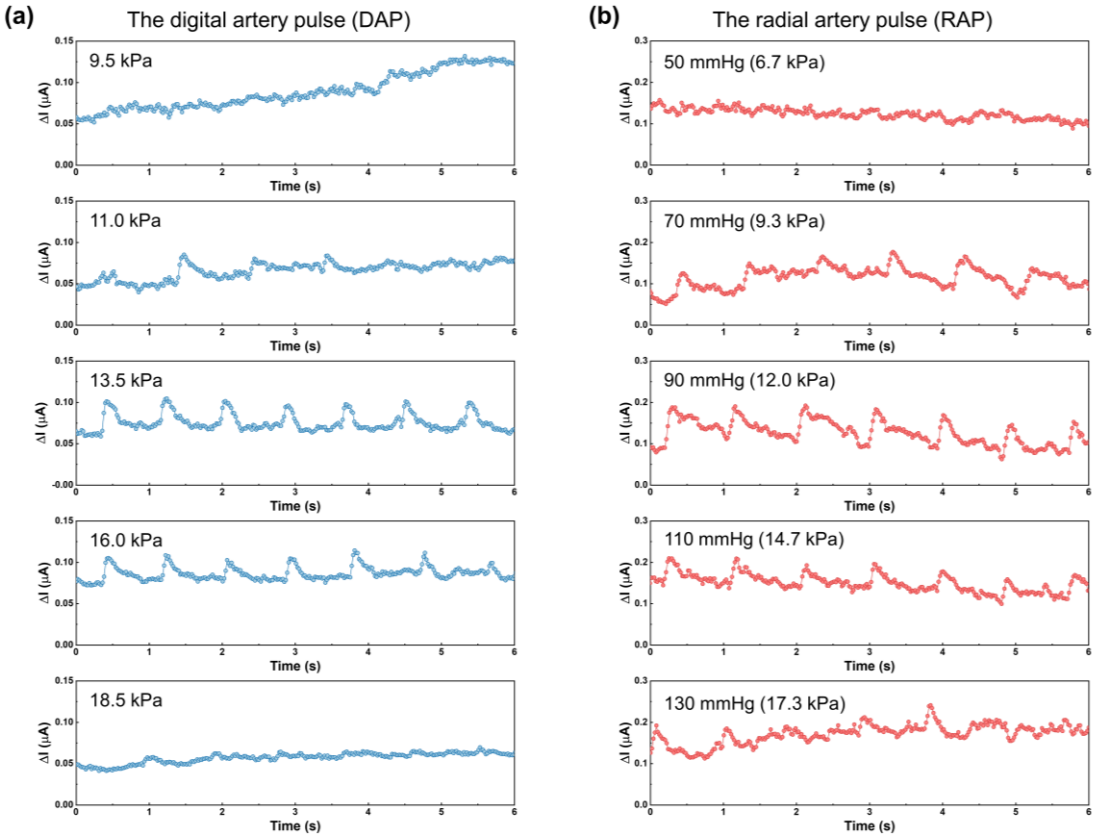

Figure S11. The pulse signals measured by MAPS under different preloads: (a) the digital artery pulse (DAP) signals and (b) the radial artery pulse (RAP) signals.

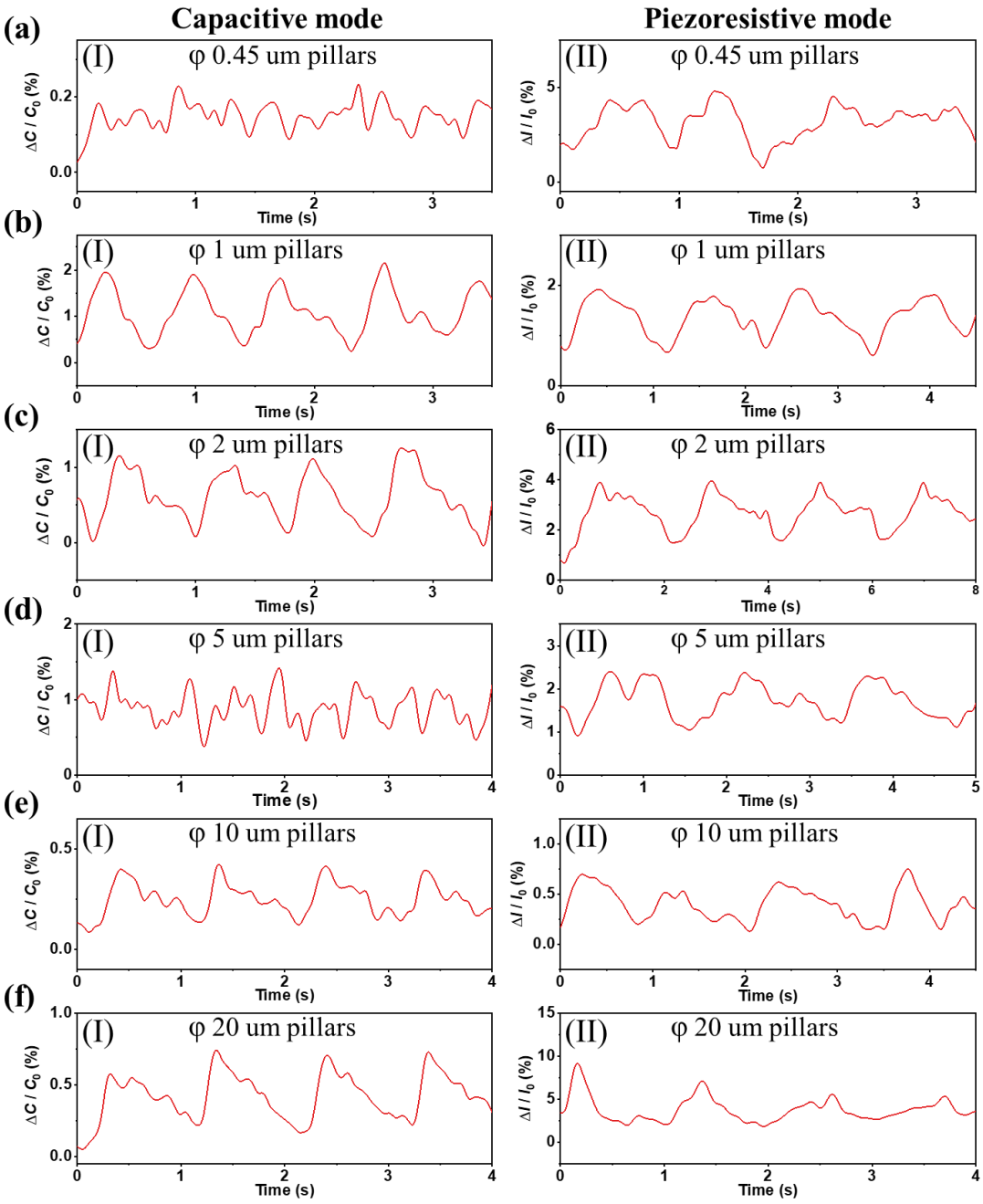

Figure S12. Pulsing sensing performance of the MAPS based on micropillar arrays with various pillar-diameters. The MAPS were fabricated in a same batch, and they were measured in both capacitive and piezoresistive modes. (a-f) Radial artery pulses monitored by the MAPS based on micropillar arrays with diameters of 0.45 μm, 1 μm, 2 μm, 5 μm, 10 μm 20 μm, respectively. Representative pulses measured in capacitive mode (I) and piezoresistive mode (II) were demonstrated. Comparative study of the results revealed that the piezoresistive mode generally output stronger pulse signals than the capacitive mode (ΔI / I_0 vs. ΔC / C_0). And the MAPS based on φ 1 μm and φ 2 μm pillars demonstrated the optimal performance, showing both good sensitivity and stability in monitoring the pulses, in both capacitive and piezoresistive modes.

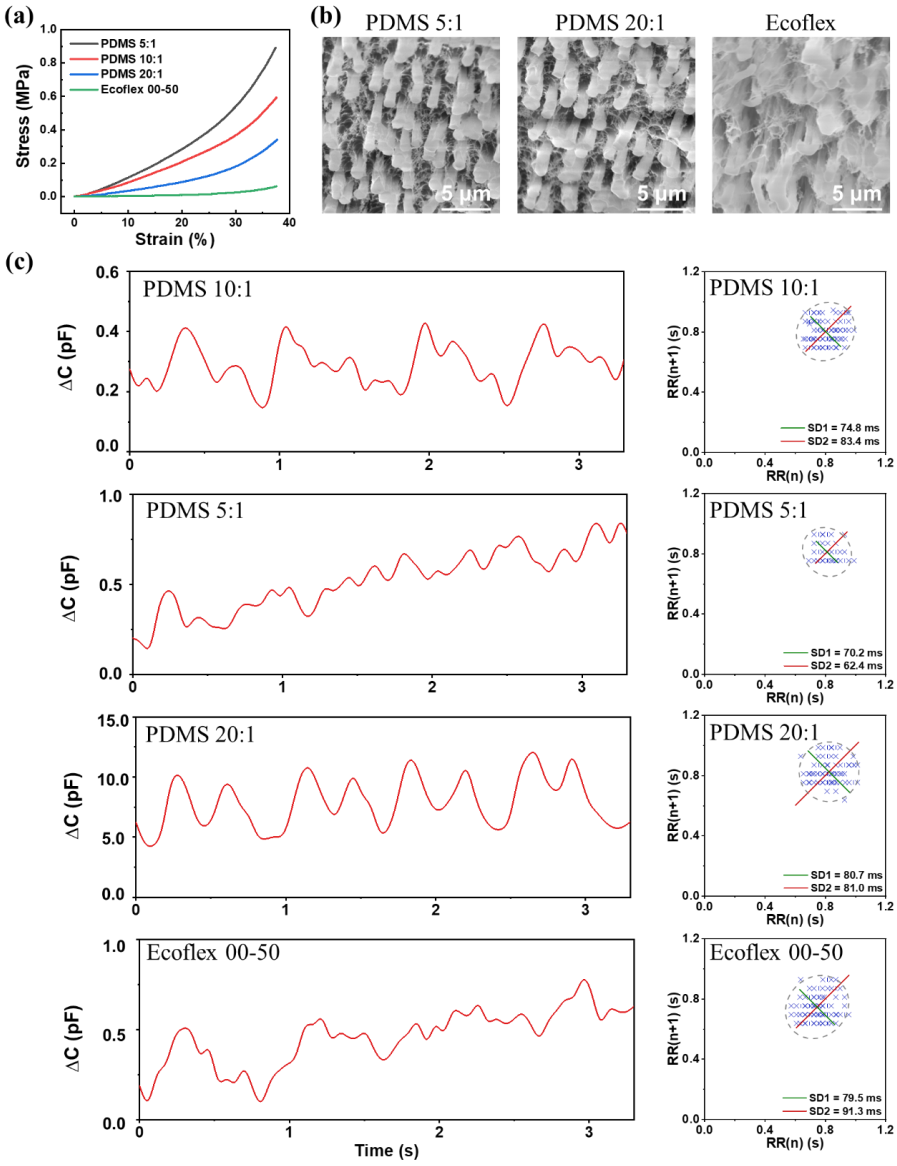

Figure S13. MAPS consist of micropillars with different modulus. Micropillars were made from 10 wt% CNT/PDMS with multiple curing conditions (ratios of PDMS and the curing agent are 5:1, 10:1 and 20:1, respectively) and 10 wt% CNT/Ecoflex (00-50). All PDMS pillars were cured at 40°C for 4 hours, and Ecoflex pillars were cured at 80°C for 1 hour as the CNT component raised curing temperature. (a) Stress-strain characterizations of the cured CNT/elastomer conductive paste. All samples for the test were fabricated and cut into a φ4 × 4 mm cylinder. (b) SEM images of micropillars with different modulus. Micropillars made from CNT/PDMS (5:1) and CNT/PDMS (20:1) showed similar morphologies as CNT/PDMS (10:1) that presented in the main text. Micropillars made from CNT/Ecoflex showed ambiguous pillar-shape, probably due to its rather low modulus. (c) Radial pulses recorded by the MAPS with different modulus and Poincare plot analysis based on the continuous pulse signals. The Poincare plot analysis widely adopted for preventing and diagnosing the heart rate variability (HRV), and flexible pressure sensors were successfully employed for analyzing the HRV in

recently years. The subject showed a healthy heart state by the Poincare plot analysis that based on the standard ECG signals, in which the SD1 = 37.1 ms, the SD2 = 70 ms, and the SD1/SD2 = 0.53. By comparing the representative pulse waves and the Poincare plot analysis, the sensor consists of CNT/PDMS (10:1) micropillars exhibited the optimal performance in pulse sensing, while the sensors consist of CNT/PDMS (5:1) and CNT/Ecoflex exhibited underperformed pulse sensing. The results indicated that the optimal sensing performance lies in a certain modulus range, pillar-materials with too high or too low modulus would lead to the deterioration of the performance.

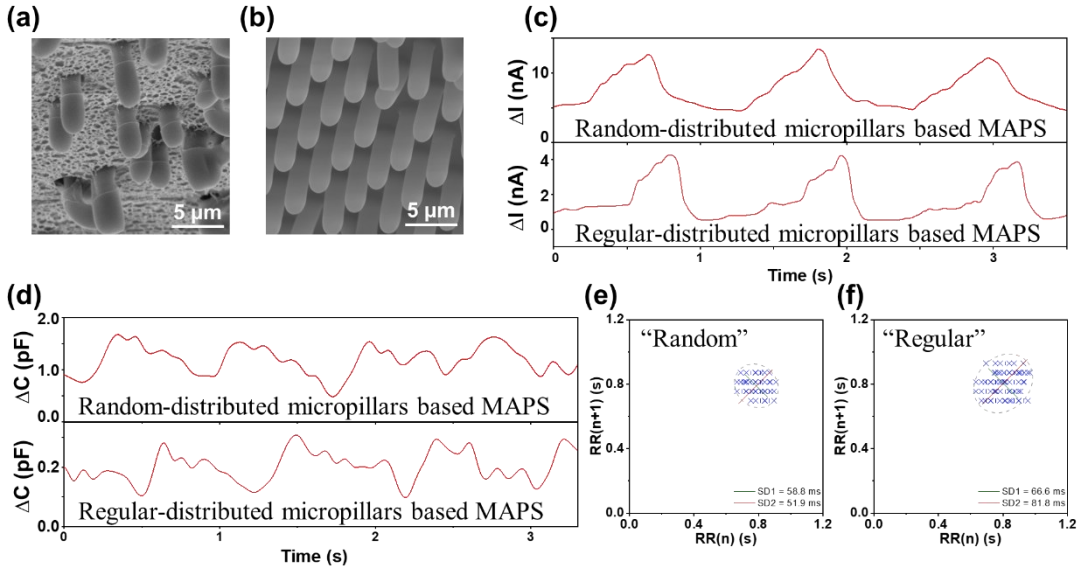

Figure S14. MAPS consist of randomly distributed and regularly distributed micropillar arrays. Randomly distribute pillars were fabricated via the process described in the manuscript, using track-etched PC membrane with the pore-size of 2 μm and the pore-density of ~2×10^6/cm^2. Regular distributed pillars were fabricated using a SU-8 template with the pore-size of 2 μm and the pore-density of ~2.7×10^6/cm^2. All pillars were made from 10 wt% CNT/PDMS mixtures that were cured at 40°C for 4 hours. SEM images of random- and regular- pillars were shown in (a) and (b), respectively. Representative pulse signals measured by random- and regular-micropillars based MAPS in the piezoresistive way (c) and the capacitive way (d) were demonstrated. Corresponding Poincare plot analysis based on the continuous pulse signals was carried out and presented in (e) and (f), respectively. The results indicate that the random or regular distribution of pillars does not significantly affect the sensing performance of pillar-based flexible pressure sensors.

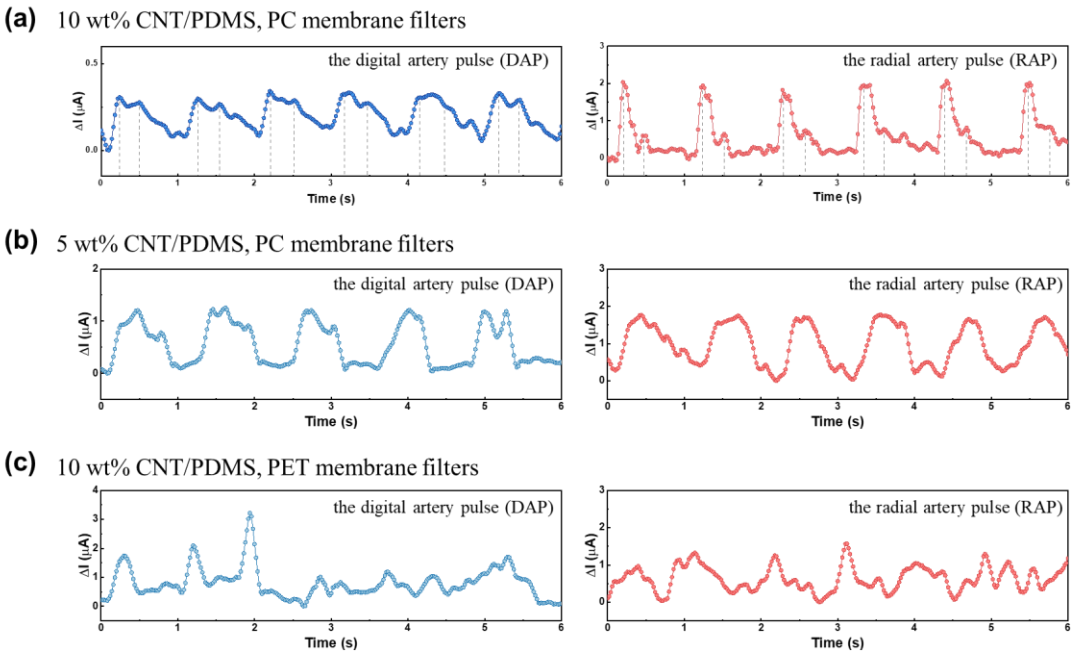

Figure S15. Representative DAP and RAP measured by the MAPS fabricated by different conductive pastes or track-etched membranes as templates. (a) MAPS fabricated using 10 wt% CNT/PDMS paste and PC membranes. Plots are the same to Figure 5c,e in the main text. (b) MAPS fabricated using 5 wt% CNT/PDMS paste and PC membranes. (c) MAPS fabricated using 10 wt% CNT/PDMS paste and PET membranes. Each measurement lasted for 1 min. All measurements were performed on one healthy subject, with at least 10-min interval between two adjacent measurements.

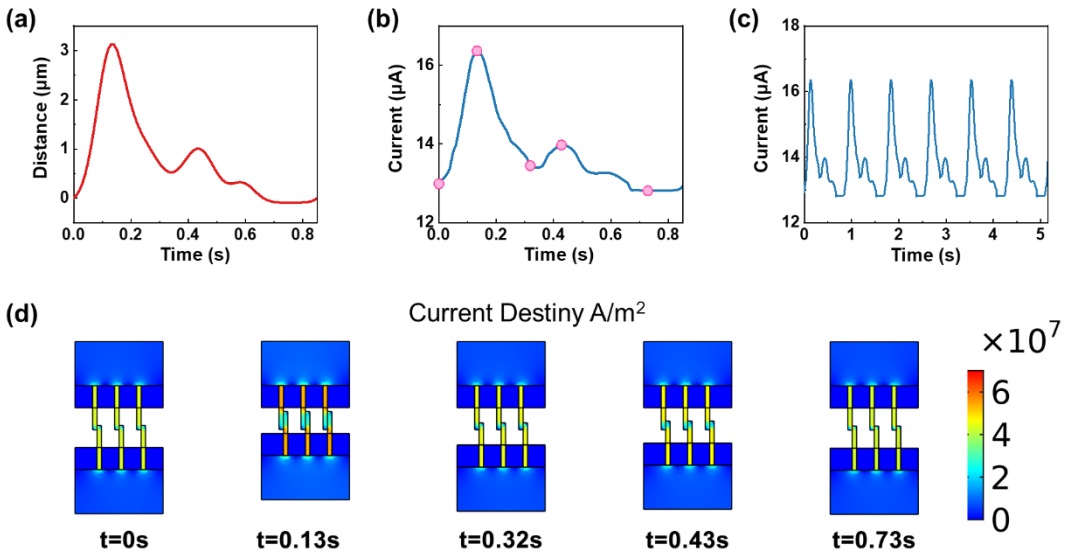

Figure S16. To further understand the sensing mechanism of arterial pulses via the MAPS, corresponding simulation model was built by COMSOL Multiphysics 5.5, for coupling the mechanical signals and the responsive electric currents. The model was simplified to a two-dimensional one, and the out-of-plane thickness was set as 100 nm. Ideally, vertical motions would not cause the deformation of micropillars, thus the upper and lower layers of the MAPS were treated as rigid domains in solid mechanical interfaces. The upper layer was fixed and the lower layer was moved according to the input of standard RAP waveforms. As the mean displacement of the RAP is ~20 μm,[1] we set the max movement distance of the lower layer to ~3 μm as the external pressure applied on the MAPS by the wrist band. As the artery pulsated, the contact area between two face-to-face pillars changed, resulting in the variation of device resistance, leading to the fluctuation of current under a constant bias (1 V). The conductivity of CNT/PDMS paste is set as 1000 S/m and the conductivity of PC membrane is set as 0.00001 S/m. (a) Standard RAP waveforms as the function of input mechanical movements of the lower layer of the MAPS. (b) An output pulse signals obtained by the simulation. (c) Continuous output pulse signals. (d) The variation of current density and pillar states along with the arterial pulsation. Each time section corresponded to the respective pink point in (b).

(1) Shao, X.; Dai, X.; Chen, Z.; He, X. Real-time 3D digital image correlation method and its application in human pulse monitoring. *Applied Optics* **2016**, *55* (4), 696-704.

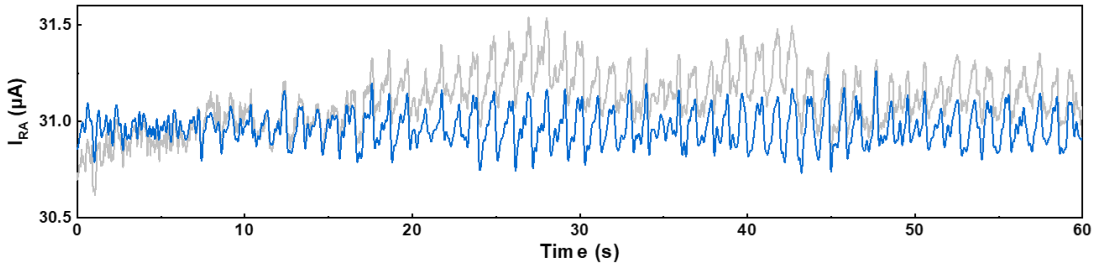

Figure S17. Signal processing of pulse signals measured by the MAPS mounted at the radial artery by medical PU tapes. The grey curve was the raw RAP signals and the blue curve was the RAP signals processed via a 0.5 – 5 Hz band-pass filter.

Figure S18. Detailed design of the flexible PCB (FPCB) for dual-pulse monitoring via the MAPS.

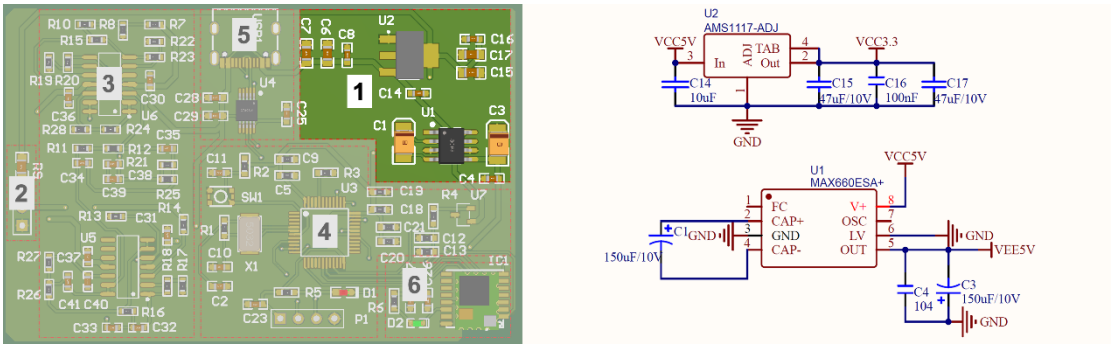

Figure S18a. Voltage conversion circuit. This circuit diagram displayed the 5 V to 3.3 V and 5 V to -5 V voltage conversion circuit (Circuit Component #1) of the FPCB. The conversion circuit, converted voltage from 5 V to 3.3 V by the voltage regulator AMS1117, provided power support for the minimum STM32 system and the Bluetooth module, and converted 5 V to −5 V by the MAX660 to power the operational amplifiers OPA4227.

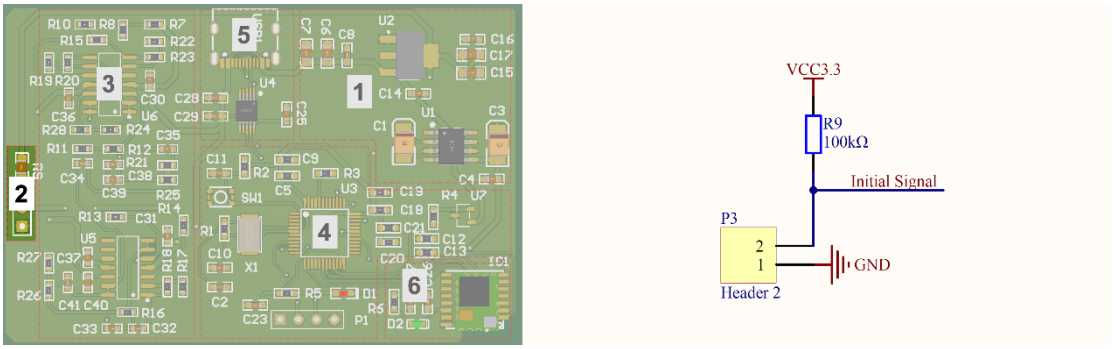

Figure S18b. The sensor interface circuit. This circuit diagram displayed the sensor interface circuit (Circuit Component #2). Deploy a suitable voltage divider on the board according to the initial resistance of the MAPS (~20 to 200 kΩ). The MAPS was electrically connected to the circuit interface, and the collected physiological signals were transmitted to the circuit interface for processing.

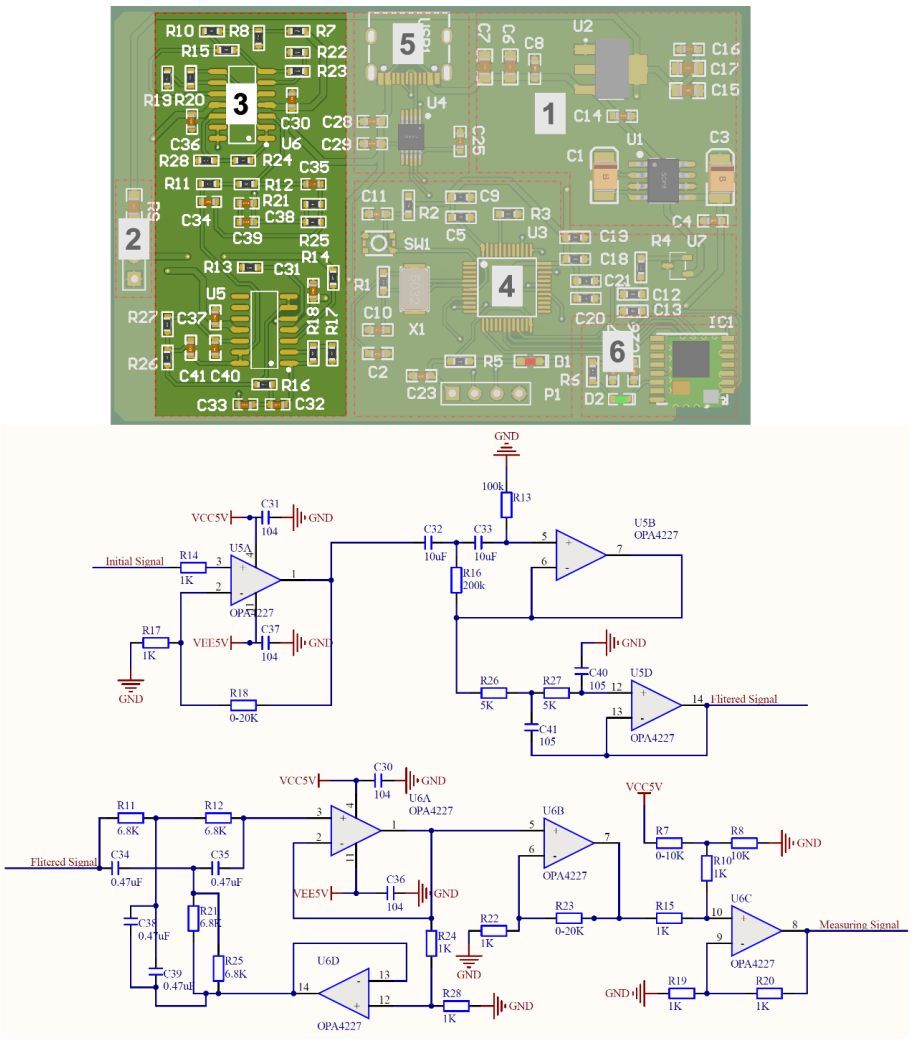

Figure S18c. The amplifier and filter circuit. This circuit diagram displayed the amplifier and filter circuit (Circuit Component #3). The circuit, at the top of the diagram, essentially made up of three operational amplifiers OPA4227, was adopted to amplify and bandpass filter the initial signal. The circuit, at the bottom of the circuit diagram, essentially made up of four operational amplifiers OPA4227, provided abilities to filter the power frequency noise, amplify the signal, and boost the voltage baseline in this work.

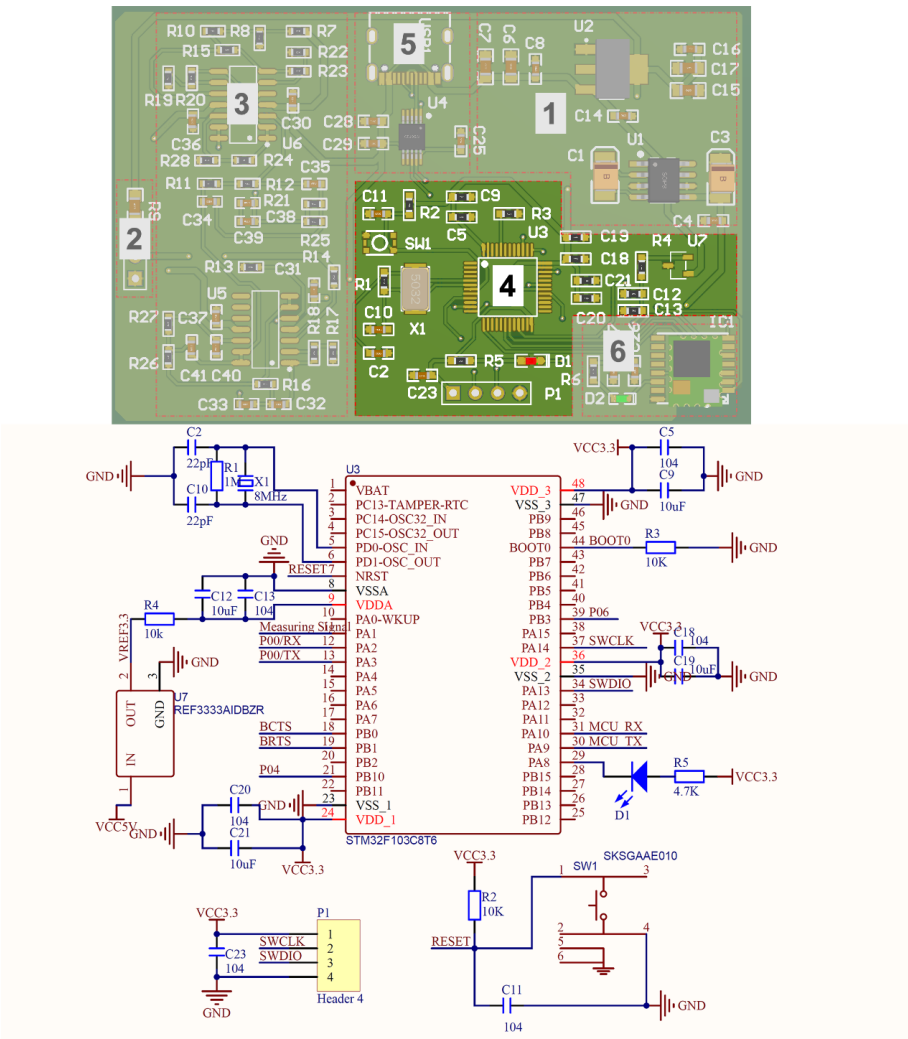

Figure S18d. The STM32 minimum system. This circuit diagram displayed the STM32 minimum system (Circuit Component #4). The STM32 minimum was composited of MCU (STM32F103C8T6), power supply circuit, clock circuit, reset circuit, debugging circuit, and reference voltage (3.3 V) converted by the REF33333AIDBZR. The STM32 minimum system can control the operation of other components in the circuit and performs preliminary processing of the data.

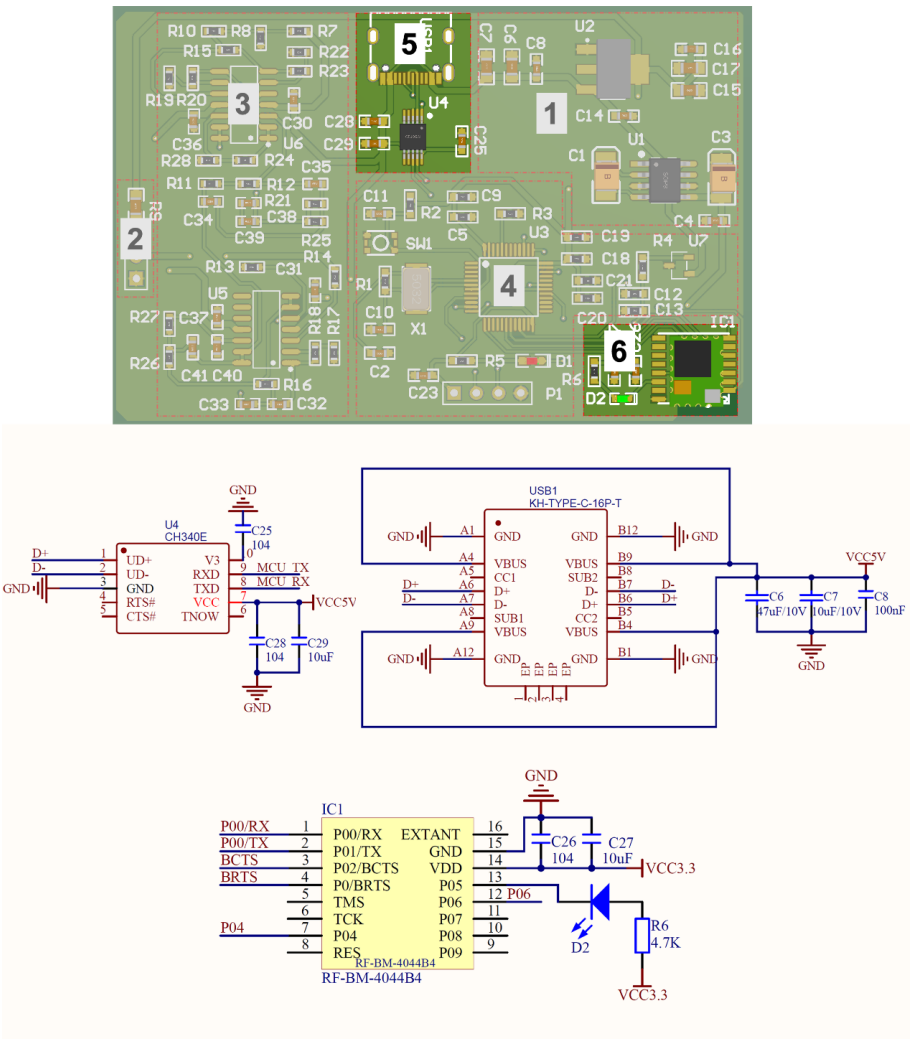

Figure S18e. The serial circuit and Bluetooth module. This circuit diagram displayed the serial port (Circuit Component #5) and the Bluetooth module (Circuit Component #6). They enabled wired and wireless physiological signals transmission between the upper and lower computers.

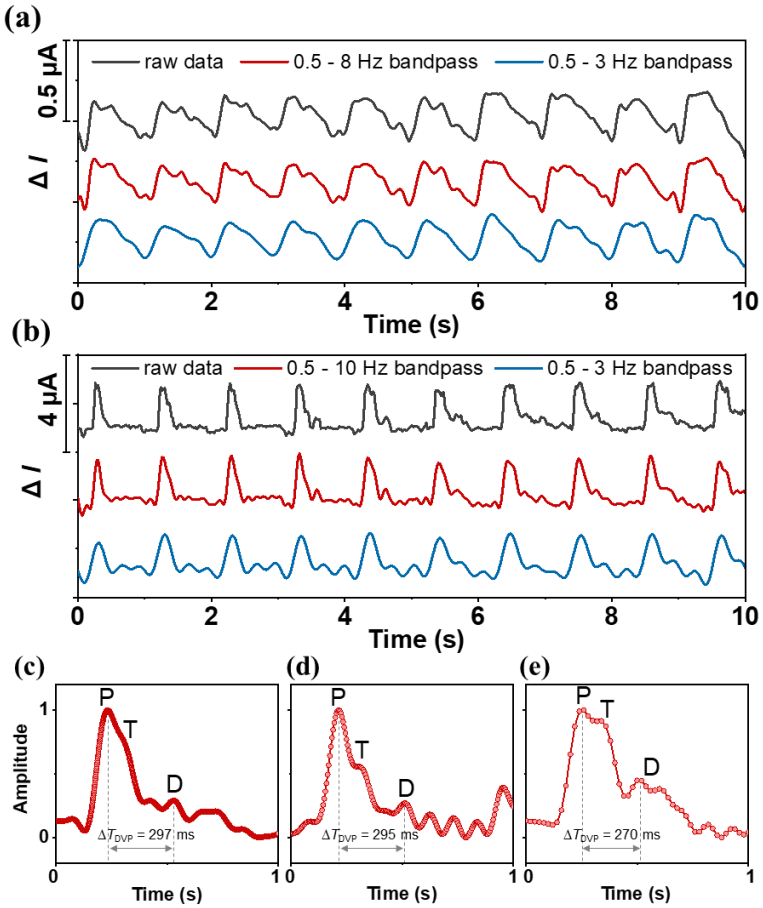

Figure S19. Enhancing the signal-quality of pulse waves. First, direct-output data of collected DAP (a) and RAP (b) showed in **Figure 5c,e** were processed by the software (OriginLab or Matlab). Bandpass filters (0.5 – 8 Hz, 0.5 – 3 Hz) were employed to filter noised at high and low frequencies. Processed pulse signals exhibited higher signal-to-noise ratio, while they partially lost details. Lower cutoff freq. of 0.3 – 0.5 Hz and upper cutoff freq. of 8 – 10 Hz were proved to be a reasonable range for applying bandpass filters on these data. Second, higher sampling rates were utilized for enhancing the signal-quality. Representative RAP waves collected using 50 Hz, 200 Hz and 1 kHz were showed in (c-e), respectively. Smoother signals were obtained at 200 Hz and 1 kHz, while signals obtained at 50 Hz also clearly exhibited key features of the pulse wave (P, T, D) and similar ΔT_{DVP}. In (c-e), pulses were collected at the same preload (> 10 kPa) and processed by the bandpass filter (0.5 – 10 Hz).

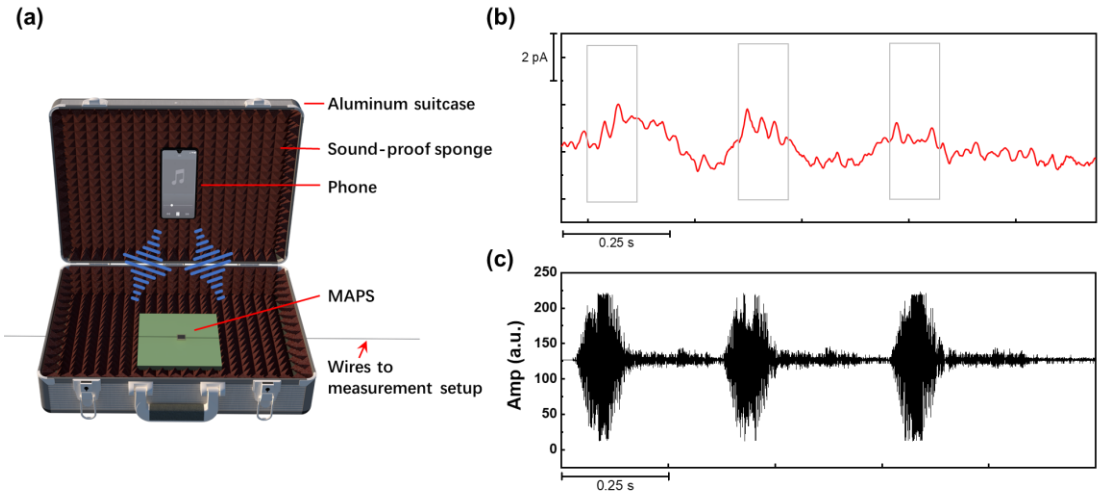

Figure S20. (a) Schematic of the experimental setup. (b) Audio playbacks recorded via MAPS in a sound-proof box. (c) The original waveform of the audio playbacks.

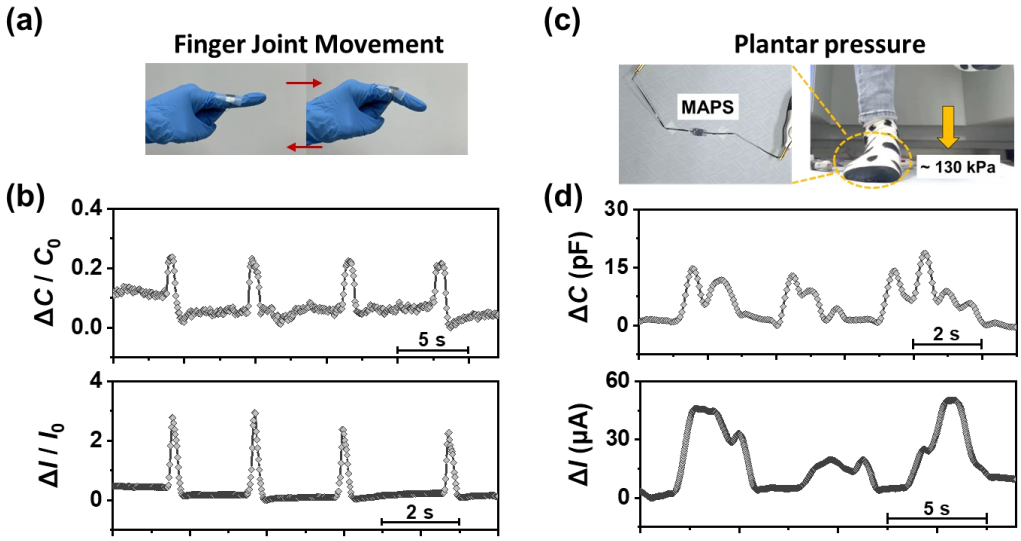

Figure S21. (a) Photographs of monitoring finger joint movement by the MAPS. (b) Collected capacitive and piezoresistive signals during the repetitive finger motions. (c) Photographs of detecting plantar pressure by the MAPS. The MAPS was fixed on the floor and a 42-kg subject repetitively stepped on the sensor with the forefoot. The pressure was gauged by the force meter afterwards. (d) Capacitive and piezoresistive signals generated by the repetitive stepping.